

# Behaviour of the Dam-Break Problem for the Serre Equations

Jordan Pitt,<sup>1</sup>  
Christopher Zoppou,<sup>1</sup>  
Stephen G. Roberts,<sup>1</sup>

## ABSTRACT

**Keywords:** dispersive waves, conservation laws, Serre equation, finite volume method, finite difference method

## INTRODUCTION

## SERRE EQUATIONS

The Serre equations can be derived as an approximation to the full Euler equations by depth integration similar to (Su and Gardner 1969). They can also be seen as an asymptotic expansion to the Euler equations as well (Lannes and Bonneton 2009). The former is more consistent with the perspective from which numerical methods will be developed while the latter indicates the appropriate regions in which to use these equations as a model for fluid flow. The set up of the scenario under which the Serre approximation is made consists of a two dimensional  $\mathbf{x} = (x, z)$  fluid over a bottom topography as in Figure 1 acting under gravity. Consider a fluid particle at depth  $\xi(\mathbf{x}, t) = z - h(x, t) - z_b(x)$  below the water surface, see Figure 1. Where the water depth is  $h(x, t)$  and  $z_b(x)$  is the bed elevation. The fluid particle is subject to the pressure,  $p(\mathbf{x}, t)$  and gravitational acceleration,  $\mathbf{g} = (0, g)^T$  and has a velocity  $\mathbf{u} = (u(\mathbf{x}, t), w(\mathbf{x}, t))$ , where  $u(\mathbf{x}, t)$  is the velocity in the  $x$ -coordinate and  $w(\mathbf{x}, t)$  is the velocity in the  $z$ -coordinate and  $t$  is time. Assuming that  $z_b(x)$  is constant the Serre equations read (Li et al. 2014)

$$\frac{\partial h}{\partial t} + \frac{\partial(\bar{u}h)}{\partial x} = 0 \quad (1a)$$

---

<sup>1</sup>Mathematical Sciences Institute, Australian National University, Canberra, ACT 0200, Australia, E-mail: Jordan.Pitt@anu.edu.au. The work undertaken by the first author was supported financially by an Australian National University Scholarship.

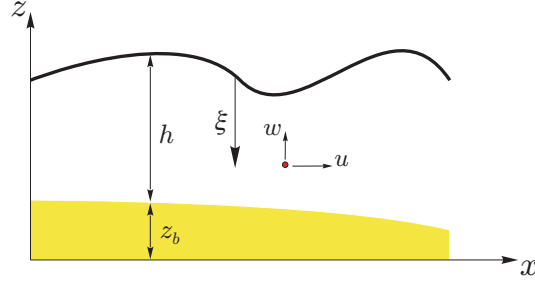


FIG. 1: The notation used for one-dimensional flow governed by the Serre equation.

$$\underbrace{\frac{\partial(\bar{u}h)}{\partial t} + \frac{\partial}{\partial x} \left( \bar{u}^2 h + \frac{gh^2}{2} \right)}_{\text{Shallow Water Wave Equations}} + \underbrace{\frac{\partial}{\partial x} \left( \frac{h^3}{3} \left[ \frac{\partial \bar{u}}{\partial x} \frac{\partial \bar{u}}{\partial x} - \bar{u} \frac{\partial^2 \bar{u}}{\partial x^2} - \frac{\partial^2 \bar{u}}{\partial x \partial t} \right] \right)}_{\text{Dispersion Terms}} = 0. \quad (1b)$$

Serre Equations

Where  $\bar{u}$  means the average of  $u$  over the depth of water.

## DIRECT NUMERICAL METHODS

Due to the presence of the mixed spatial and temporal derivatives in the conservation of momentum equation (1b) the choices of methods for these particular equations are limited. Thus the two direct numerical methods presented in this paper will begin by approximating (1b) by finite differences. To facilitate this a uniform grid in space will be used with  $\Delta x = x_{i+1} - x_i$  for all  $i$  and quantities evaluated at these grid points will be denoted by subscripts for example  $h_i = h(x_i)$ . The grid in time will be denoted by superscripts for example  $h^n = h(t^n)$ , noting that  $h^n$  is a function in space.

### Finite Difference Appximation to Conservation of Momentum Equation

In [[Zoppou thesis/my work]] it was demonstrated that an efficient numerical scheme for the Serre equations must be at least second-order accurate thus the derivatives in (1b) will be approximated by second-order finite differences. Firstly (1b) must be expanded, making use of (1a) one obtains

$$h \frac{\partial u}{\partial t} + X - h^2 \frac{\partial^2 u}{\partial x \partial t} - \frac{h^3}{3} \frac{\partial^3 u}{\partial x^2 \partial t} = 0 \quad (2a)$$

where  $X$  contains only spatial derivatives and is

$$X = uh \frac{\partial u}{\partial x} + gh \frac{\partial h}{\partial x} + h^2 \frac{\partial u}{\partial x} \frac{\partial u}{\partial x} + \frac{h^3}{3} \frac{\partial u}{\partial x} \frac{\partial^2 u}{\partial x^2} - h^2 u \frac{\partial^2 u}{\partial x^2} - \frac{h^3}{3} u \frac{\partial^3 u}{\partial x^3} \quad (2b)$$

where the bar over  $u$  has been dropped to simplify notation. Then taking second-order centred finite difference approximation to the time derivatives for (2a) gives

$$h^n \frac{u^{n+1} - u^{n-1}}{2\Delta t} + X^n - (h^n)^2 \frac{\left(\frac{\partial u}{\partial x}\right)^{n+1} - \left(\frac{\partial u}{\partial x}\right)^{n-1}}{2\Delta t} - \frac{(h^n)^3}{3} \frac{\left(\frac{\partial^2 u}{\partial x^2}\right)^{n+1} - \left(\frac{\partial^2 u}{\partial x^2}\right)^{n-1}}{2\Delta t} = 0,$$

$$h^n (u^{n+1} - u^{n-1}) + 2\Delta t X^n - (h^n)^2 \left( \left(\frac{\partial u}{\partial x}\right)^{n+1} - \left(\frac{\partial u}{\partial x}\right)^{n-1} \right) - \frac{(h^n)^3}{3} \left( \left(\frac{\partial^2 u}{\partial x^2}\right)^{n+1} - \left(\frac{\partial^2 u}{\partial x^2}\right)^{n-1} \right) = 0.$$

Introducing

$$Y^n = 2\Delta t X^n - h^n u^{n-1} + (h^n)^2 \left(\frac{\partial u}{\partial x}\right)^{n-1} + \frac{(h^n)^3}{3} \left(\frac{\partial^2 u}{\partial x^2}\right)^{n-1}$$

and rearranging results in

$$h^n u^{n+1} - (h^n)^2 \left(\frac{\partial u}{\partial x}\right)^{n+1} - \frac{(h^n)^3}{3} \left(\frac{\partial^2 u}{\partial x^2}\right)^{n+1} + Y^n = 0.$$

Taking second-order approximations to the spatial derivatives and evaluating the quantities at the correct locations gives

$$h_i^n u_i^{n+1} - (h_i^n)^2 \left( \frac{u_{i+1}^{n+1} - u_{i-1}^{n+1}}{2\Delta x} \right) - \frac{(h_i^n)^3}{3} \left( \frac{u_{i+1}^{n+1} - 2u_i^{n+1} + u_{i-1}^{n+1}}{\Delta x^2} \right) = -Y_i^n \quad (3)$$

This can be rearranged into a tri-diagonal matrix that updates  $u$  given its current and previous values. So that

$$\begin{bmatrix} u_0^{n+1} \\ \vdots \\ u_m^{n+1} \end{bmatrix} = A^{-1} \begin{bmatrix} -Y_0^n \\ \vdots \\ -Y_m^n \end{bmatrix} =: \mathcal{G}_u(u^n, h^n, u^{n-1}, h^{n-1}, \Delta x, \Delta t). \quad (4)$$

Where

$$A = \begin{bmatrix} b_0 & c_0 & & & & \\ a_0 & b_1 & c_1 & & & \\ & a_1 & b_2 & c_2 & & \\ & & \ddots & \ddots & \ddots & \\ & & & a_{m-3} & b_{m-2} & c_{m-2} \\ & & & & a_{m-2} & b_{m-1} & c_{m-1} \\ & & & & & a_{m-1} & b_m \end{bmatrix}$$

with

$$a_{i-1} = \frac{(h_i^n)^2}{2\Delta x} \frac{h_{i+1}^n - h_{i-1}^n}{2\Delta x} - \frac{(h_i^n)^3}{3\Delta x^2}, \quad (5a)$$

$$b_i = h_i^n + \frac{2h_i^n}{3\Delta x^2} \quad (5b)$$

and

$$c_i = -\frac{(h_i^n)^2}{2\Delta x} \frac{h_{i+1}^n - h_{i-1}^n}{2\Delta x} - \frac{(h_i^n)^3}{3\Delta x^2}. \quad (5c)$$

64 Lastly for completeness the final expression for  $Y_i^n$  is given by

$$\begin{aligned} Y_i^n = & 2\Delta t \left[ u_i^n h_i^n \frac{u_{i+1}^n - u_{i-1}^n}{2\Delta x} + g h_i^n \frac{h_{i+1}^{n-1} - h_{i-1}^{n-1}}{2\Delta x} + (h_i^n)^2 \left( \frac{u_{i+1}^{n-1} - u_{i-1}^{n-1}}{2\Delta x} \right)^2 \right. \\ & + \frac{(h_i^n)^3}{3} \frac{u_{i+1}^n - u_{i-1}^n}{2\Delta x} \frac{u_{i+1}^n - 2u_i^n + u_{i-1}^n}{\Delta x^2} - (h_i^n)^2 u_i^n \frac{u_{i+1}^n - 2u_i^n + u_{i-1}^n}{\Delta x^2} \\ & - \frac{(h_i^n)^3}{3} u_i^n \frac{u_{j+2}^n - 2u_{j+1}^n + 2u_{j-1}^n - u_{j-2}^n}{2\Delta x^3} \left. \right] \\ & - h_i^n u_i^{n-1} + (h_i^n)^2 \frac{u_{i+1}^{n-1} - u_{i-1}^{n-1}}{2\Delta x} + \frac{(h_i^n)^3}{3} \frac{u_{i+1}^{n-1} - 2u_i^{n-1} + u_{i-1}^{n-1}}{\Delta x^2}. \end{aligned} \quad (6)$$

65  
66  
67 In particular this is an explicit numerical method for (1b), that requires the current and  
68 previous values of  $h$  and  $u$ .

### 69 The Lax Wendroff Method for Conservation of Mass Equation

70 Because the conservation of mass equation (1a) has no mixed derivative term a wider  
71 range of numerical methods can be used. This paper will use two, one using the Lax  
72 Wendroff method as was done by El et al. (2006) and the other will use the same process  
73 as []. Both of these are theoretically second-order accurate. To make these methods precise  
74 they will be presented here in sufficient replicable detail.

75 Note that (1a) is in conservative law form for  $h$  where the Jacobian is  $u$ . Thus using  
76 the previously defined spatio-temporal discretisation the lax-wendroff update for  $h$  is

$$\begin{aligned} h_i^{n+1} = & h_i^n - \frac{\Delta t}{2\Delta x} ((uh)_{i+1}^n - (uh)_{i-1}^n) \\ & + \frac{\Delta t^2}{2\Delta x^2} \left( \frac{u_{i+1}^n - u_i^n}{2} ((uh)_{i+1}^n - (uh)_i^n) - \frac{u_i^n - u_{i-1}^n}{2} ((uh)_i^n - (uh)_{i-1}^n) \right). \end{aligned} \quad (7)$$

77  
78  
79 Performing this update for all  $i$  will be denoted by  $\mathcal{E}_h(\mathbf{u}^n, \mathbf{h}^n, \Delta x, \Delta t)$ .

## 80 Second Order Finite Difference Method

81 To follow the process above [] to obtain a second-order finite difference approximation  
82 to (1a) the derivatives are first expanded then approximated by second order centered finite  
83 differences to give

$$84 \frac{h_i^{n+1} - h_i^{n-1}}{2\Delta t} + u_i^n \frac{h_{i+1}^n - h_{i-1}^n}{2\Delta x} + h_i^n \frac{u_{i+1}^n - u_{i-1}^n}{2\Delta x} = 0. \quad (8)$$

86 After rearranging this to give an update formula one obtains

$$87 h_i^{n+1} = h_i^{n-1} - \Delta t \left( u_i^n \frac{h_{i+1}^n - h_{i-1}^n}{\Delta x} + h_i^n \frac{u_{i+1}^n - u_{i-1}^n}{\Delta x} \right). \quad (9)$$

89 Performing this update for all  $i$  will be denoted by  $\mathcal{G}_h(\mathbf{u}^n, \mathbf{h}^n, \mathbf{h}^{n-1}, \Delta x, \Delta t)$ .

## 90 The Finite Difference Methods

91 To summarise the first numerical method which naively approximates all derivatives  
92 by finite differences has the following update algorithm

$$93 \left. \begin{aligned} \mathbf{h}^{n+1} &= \mathcal{G}_h(\mathbf{u}^n, \mathbf{h}^n, \Delta x, \Delta t) \\ \mathbf{u}^{n+1} &= \mathcal{G}_u(\mathbf{u}^n, \mathbf{h}^n, \mathbf{u}^{n-1}, \mathbf{h}^{n-1}, \Delta x, \Delta t) \end{aligned} \right\} \mathcal{G}(\mathbf{u}^n, \mathbf{h}^n, \mathbf{u}^{n-1}, \mathbf{h}^{n-1}, \Delta x, \Delta t). \quad (10)$$

95 While the second method which follows from a naive interpretation of the numerical  
96 method described by El et al. (2006) is

$$97 \left. \begin{aligned} \mathbf{h}^{n+1} &= \mathcal{E}_h(\mathbf{u}^n, \mathbf{h}^n, \Delta x, \Delta t) \\ \mathbf{u}^{n+1} &= \mathcal{G}_u(\mathbf{u}^n, \mathbf{h}^n, \mathbf{u}^{n-1}, \mathbf{h}^{n-1}, \Delta x, \Delta t) \end{aligned} \right\} \mathcal{E}(\mathbf{u}^n, \mathbf{h}^n, \mathbf{u}^{n-1}, \mathbf{h}^{n-1}, \Delta x, \Delta t). \quad (11)$$

## 100 CONSERVATIVE FORM OF THE SERRE EQUATIONS

101 To overcome the aforementioned difficulty of mixed derivatives the Serre equations (1)  
102 can be reformulated into conservative form which has no mixed spatio-temporal deriva-  
103 tives. This is accomplished by the introduction of a new quantity (Le Métayer et al. 2010;  
104 Zoppou 2014)

$$105 G = uh - h^2 \frac{\partial h}{\partial x} \frac{\partial u}{\partial x} - \frac{h^3}{3} \frac{\partial^2 u}{\partial x^2}. \quad (12)$$

107 Consequently, (1) can be rewritten as

$$108 \frac{\partial h}{\partial t} + \frac{\partial(uh)}{\partial x} = 0 \quad (13a)$$

110 and

$$111 \frac{\partial G}{\partial t} + \frac{\partial}{\partial x} \left( Gu + \frac{gh^2}{2} - \frac{2h^3}{3} \frac{\partial u}{\partial x} \frac{\partial u}{\partial x} \right) = 0. \quad (13b)$$

## A Hybrid Finite Difference-Volume Method for Serre Equations in Conservative Form

The conservative form (13) allows for a wider range of numerical techniques such as finite element methods (Li et al. 2014) and finite volume methods (Le Métayer et al. 2010; Zoppou 2014). In this paper the finite volume methods will be used and so our full solution scheme  $\mathcal{H}$  will be composed of a scheme  $\mathcal{A}$  that given  $h$  and  $G$  solves (12) for  $u$  and a scheme  $\mathcal{L}$  that given all three quantities solves (13) giving  $h$  and  $G$  at some later time.

### Finite Difference Approximation for $\mathcal{A}$

In this paper the scheme  $\mathcal{A}$  will be given by approximating all the derivatives in (12) by finite differences [this was done above for second order] in particular second- and fourth-order centred finite differences and then rearranging into a matrix equation of the form

$$\begin{bmatrix} u_0 \\ \vdots \\ u_m \end{bmatrix} = A^{-1}(h) \begin{bmatrix} G_0 \\ \vdots \\ G_m \end{bmatrix} =: \mathcal{A}(h, G).$$

For a second-order approximation  $A(h)$  is tri-diagonal while for a fourth-order approximation  $A(h)$  is penta-diagonal.

### Finite Volume Method for $\mathcal{L}$

Finite volume methods work with cell averages which are the value of a quantity averaged over a cell and is denoted by a bar and a spatial subscript corresponding to the centre of the cell. For example

$$\bar{h}_i = \frac{1}{\Delta x} \int_{x_{i-\frac{1}{2}}}^{x_{i+\frac{1}{2}}} h(x, t) dx$$

is the averaged water depth in the cell with centre  $x_i$  spanning  $[x_{i-1/2}, x_{i+1/2}]$  where  $x_{i\pm 1/2} = x_i \pm \Delta x/2$ . Finite volume methods update these cell averages in time using the formula

$$\bar{U}_i^{n+1} = \bar{U}_i^n - \frac{\Delta t}{\Delta x} (F_{i+\frac{1}{2}}^n - F_{i-\frac{1}{2}}^n) \quad (14)$$

where for (13)  $\bar{U}_i^n = [\bar{h}_i^n \bar{G}_i^n]^T$  is an approximation of the vector of the conserved quantities averaged over the cell at time  $t^n$ . While  $F_{i\pm 1/2}^n$  is an approximation of the average flux over the time interval  $[t^n, t^{n+1}]$  at the respective cell boundary  $x_{i\pm 1/2}$ , which is obtained by solving a local Riemann problem at the cell boundaries. In Kurganov et al. (2002)  $F_{i\pm 1/2}^n$  is given by

$$F_{i+\frac{1}{2}} = \frac{a_{i+\frac{1}{2}}^+ f(q_{i+\frac{1}{2}}^-) - a_{i+\frac{1}{2}}^- f(q_{i+\frac{1}{2}}^+)}{a_{i+\frac{1}{2}}^+ - a_{i+\frac{1}{2}}^-} + \frac{a_{i+\frac{1}{2}}^+ a_{i+\frac{1}{2}}^-}{a_{i+\frac{1}{2}}^+ - a_{i+\frac{1}{2}}^-} [q_{i+\frac{1}{2}}^+ - q_{i+\frac{1}{2}}^-] \quad (15)$$

146 where  $f$  is the instantaneous flux of the conserved quantity  $q$  evaluated using the recon-  
 147 structed values from the cells adjacent to the cell interface  $x_{i+1/2}$ . While  $a_{i+1/2}^-$  and  $a_{i+1/2}^+$   
 148 are given by

$$149 \quad a_{i+\frac{1}{2}}^- = \min \left[ \lambda_1 \left( q_{i+\frac{1}{2}}^- \right), \lambda_1 \left( q_{i+\frac{1}{2}}^+ \right), 0 \right]$$

151 and

$$152 \quad a_{i+\frac{1}{2}}^+ = \max \left[ \lambda_2 \left( q_{i+\frac{1}{2}}^- \right), \lambda_2 \left( q_{i+\frac{1}{2}}^+ \right), 0 \right].$$

154 where  $\lambda_1 = u - \sqrt{gh}$  and  $\lambda_2 = u + \sqrt{gh}$  since it was demonstrated in Zoppou (2014) that  
 155 these are bounds on the phase speed of the Serre equations.

## 156 NUMERICAL SIMULATIONS

157 In this section the methods introduced in this paper will be validated by using them  
 158 to approximate an analytic solution of the Serre equations, this will also be used to verify  
 159 their order of accuracy. Then an in depth comparison of using these methods for a smooth  
 160 approximation to the discontinuous dam break problem will be provided to investigate the  
 161 behaviour of these equations in the presence of discontinuities. This is a problem that so  
 162 far has only received a proper treatment in (El et al. 2006), with other research giving only  
 163 a cursory look into the topic.

## 164 SOLITON

165 Currently cnoidal waves are the only family of analytic solutions to the Serre equa-  
 166 tions (Carter and Cienfuegos 2011). Solitons are a particular instance of cnoidal waves  
 167 that travel without deformation and have been used to verify the convergence rates of the  
 168 described methods in this paper.

169 For the Serre equations the solitons have the following form

$$170 \quad h(x, t) = a_0 + a_1 \operatorname{sech}^2(\kappa(x - ct)), \quad (16a)$$

$$173 \quad u(x, t) = c \left( 1 - \frac{a_0}{h(x, t)} \right), \quad (16b)$$

$$176 \quad \kappa = \frac{\sqrt{3a_1}}{2a_0 \sqrt{a_0 + a_1}} \quad (16c)$$

178 and

$$179 \quad c = \sqrt{g(a_0 + a_1)} \quad (16d)$$

180  
181 where  $a_0$  and  $a_1$  are input parameters that determine the depth of the quiescent water and  
182 the maximum height of the soliton above that respectively. In the simulation  $a_0 = 10\text{m}$ ,  
183  $a_1 = 1\text{m}$  for  $x \in [-500\text{m}, 1500\text{m}]$  and  $t \in [0\text{s}, 100\text{s}]$ . With  $\Delta t = 0.01\Delta x$  which satisfies []  
184 and  $\theta = 1.2$  for the second-order finite difference-volume method.

## 185 **SMOOTHED DAM-BREAK**

186 The discontinuous dam-break problem can be approximated by a smooth function using  
187 the hyperbolic tangent function. Such an approximation will be called a smoothed  
188 dam-break problem and will be defined as such

$$189 \quad h(x, 0) = h_0 + \frac{h_1 - h_0}{2} (1 + \tanh(\alpha(x_0 - x))), \quad (17a)$$

$$190 \quad u(x, 0) = 0.0\text{m/s}. \quad (17b)$$

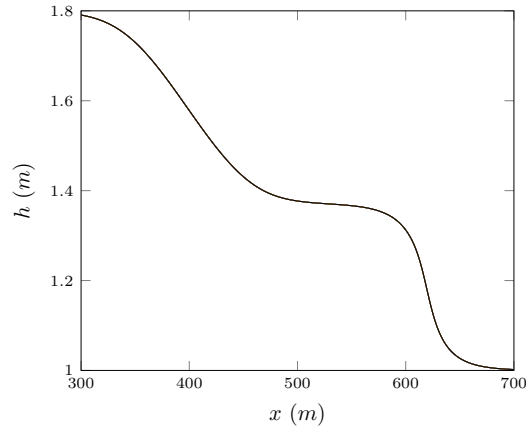
191  
192  
193  
194 Where  $a$  is given and controls the width of the transition between the two dam-break  
195 heights of  $h_0$  and  $h_1$ . For large  $\alpha$  the width is small and vice versa. For a fixed  $\Delta x$  there  
196 are large enough  $\alpha$  values such that the transition width is zero. This experiment was run  
197 for both of the methods described in this paper and the 3 different order finite difference-  
198 volume methods described in []. In this particular simulation  $h_0 = 1.0\text{m}$ ,  $h_1 = 1.8\text{m}$  on  
199  $x \in [0\text{m}, 1000\text{m}]$  for  $t \in [0\text{s}, 30\text{s}]$  with  $x_0 = 500\text{m}$ . The simulations were run changing  
200 both  $\Delta x$  and  $\alpha$  and for stability  $\Delta t = 0.01\Delta x$  while for the second-order finite volume  
201 method  $\theta = 1.2$ . Since this experiment involves a very large amount of data the analysis  
202 will be broken up into three sections: decreasing  $\Delta x$ , increasing  $\alpha$  and finally differences  
203 between the methods.

## 204 **Changing $\Delta x$**

205 Decreasing  $\Delta x$  allows the numerical method to better approximate the analytic solution  
206 to the equations. So for our valid [] numerical methods it would be expected that smaller  
207  $\Delta x$ 's provide a closer approximation to the analytic solution This was demonstrated for  
208 smooth problems [] above.

209 In this comparison we pick an  $\alpha$  and a method and investigate the result of decreasing  
210  $\Delta x$ . Because the smoothness of the initial conditions depends on both  $\Delta x$  and  $\alpha$  one must  
211 be careful that the initial conditions do not change from discontinuous to smooth as  $\Delta x$  is  
212 altered as then we are no longer comparing smooth problems. This is of particular impor-  
213 tance for the two finite difference methods as they do not correctly handle discontinuos  
214 initial conditions. []





(a)

FIG. 2: Smooth dam break problem for  $\alpha = 0.025$  for  $\Delta x = 10/2^{10}$  (blue),  $\Delta x = 10/2^9$  (green),  $\Delta x = 10/2^8$  (red),  $\Delta x = 10/2^7$  (cyan),  $\Delta x = 10/2^6$  (magenta),  $\Delta x = 10/2^5$  (yellow),  $\Delta x = 10/2^4$  (black)

215 The first and most important observation is that there are four types of behaviour as  
 216  $\Delta x \rightarrow 0$  of the problem depending on the  $\alpha$  and the numerical method. It was found  
 217 that the second- and third-order methods had similar  $\alpha$  ranges determining the trending  
 218 behaviour while the first-order had very different ranges, because of this large difference  
 219 the term higher-order will be used to refer to all second- and third- order methods. Also  
 220 for the purposes of simplicity these scenario's will be demonstrated by solutions of the  
 221 FDVM as they are better for illustrative purposes. The four scenarios are identified by the  
 222 behaviour of the solutions when  $\Delta x$  is small and they correspond to different results in the  
 223 literature.

224 The first behaviour which will be referred to as the non-oscillatory scenario has such  
 225 smooth initial conditions that there are no introduced oscillations. This scenario ends at  
 226  $\alpha = 0.025$  and should in theory extend down to the trivial  $\alpha = 0$ , in these ranges the  
 227 smoothed dam-break problem is a very poor approximation to the dam-break problem.  
 228 This behaviour was observed for all methods when  $\alpha = 0.025$  and an example case for the  
 229 third-order method is plotted in Figure 2. This example demonstrates rapid convergence  
 230 with all the solutions being graphically identical. This scenario resembles the solution of  
 231 the shallow water wave equations in that it contains only a rarefaction and a shock with no  
 232 dispersion.

233 The second will be referred to as the flat scenario due to the presence of a con-  
 234 stant height state between the oscillations at the shock and rarefaction fan. This scenario

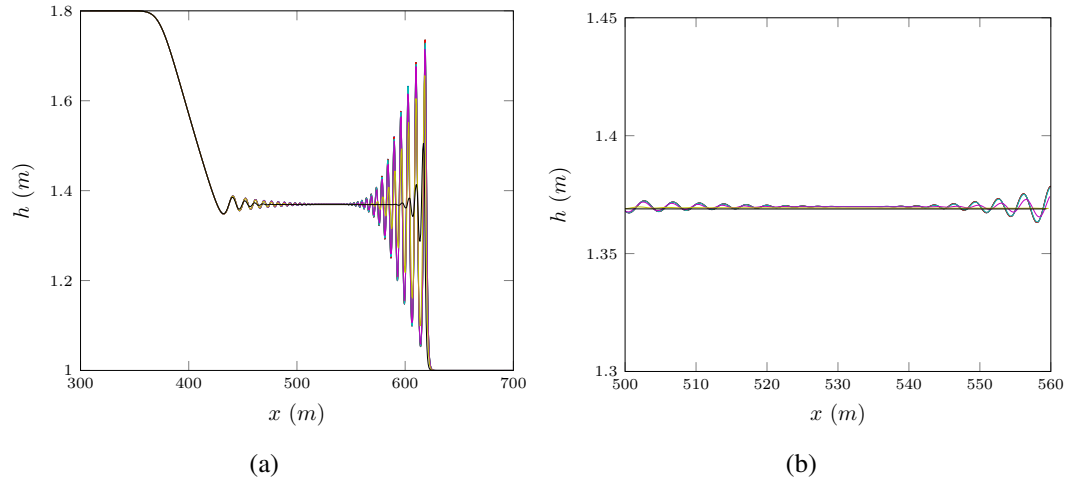


FIG. 3: Smooth dam break problem for o3 [] with  $\alpha = 0.5$  for  $\Delta x = 10/2^{10}$  (blue),  $\Delta x = 10/2^9$  (green),  $\Delta x = 10/2^8$  (red),  $\Delta x = 10/2^7$  (cyan),  $\Delta x = 10/2^6$  (magenta),  $\Delta x = 10/2^7$  (yellow),  $\Delta x = 10/2^8$  (black)

emerges at  $\alpha = 0.05$  and continues to  $\alpha = 1$  for the higher-order methods and occurs from  $\alpha = 0.05$  to  $\alpha = 1000$  for the first-order method (so far). This scenario corresponds to the results presented by Le Métayer et al. (2010) and Mitsotakis et al. (2014).

An example plot demonstrating this scenario for the third-order method with  $\alpha = 0.5$  can be seen in Figure 3. As  $\Delta x$  decreases the solutions converge which is sensible since for the  $\Delta x$  in Figure [] the initial conditions are smooth as can be seen in Figure [] and these methods have been verified for smooth problems. So that by  $\Delta x = 10/2^8$  the solutions for higher  $\Delta x$  are graphically identical.

The third scenario will be referred to as the contact discontinuity scenario due to the use of that term to describe it by El et al. (2006). For the higher-order methods it occurs at  $\alpha = 2.5$  and so far has not occurred for the first order method[]. The contact discontinuity scenarios main feature is that the oscillations from the rarefaction fan and the shock decay and appear to meet at a point as can be seen in Figure 4. For the experiments performed this doesn't appear to be an actual centre point but rather that the oscillations decay so quickly around the 'contact discontinuity' that it appears to be the case. All the higher order methods so far have not shown a converged solution as  $\Delta x$  decreases. However it does appear that convergence is likely with the solutions getting closer together.

The fourth scenario will be referred to as the bump scenario due to the oscillations no longer decaying down towards a point but rather growing around where the contact discontinuity was in the previous scenario as can be seen in Figure 5. This behaviour

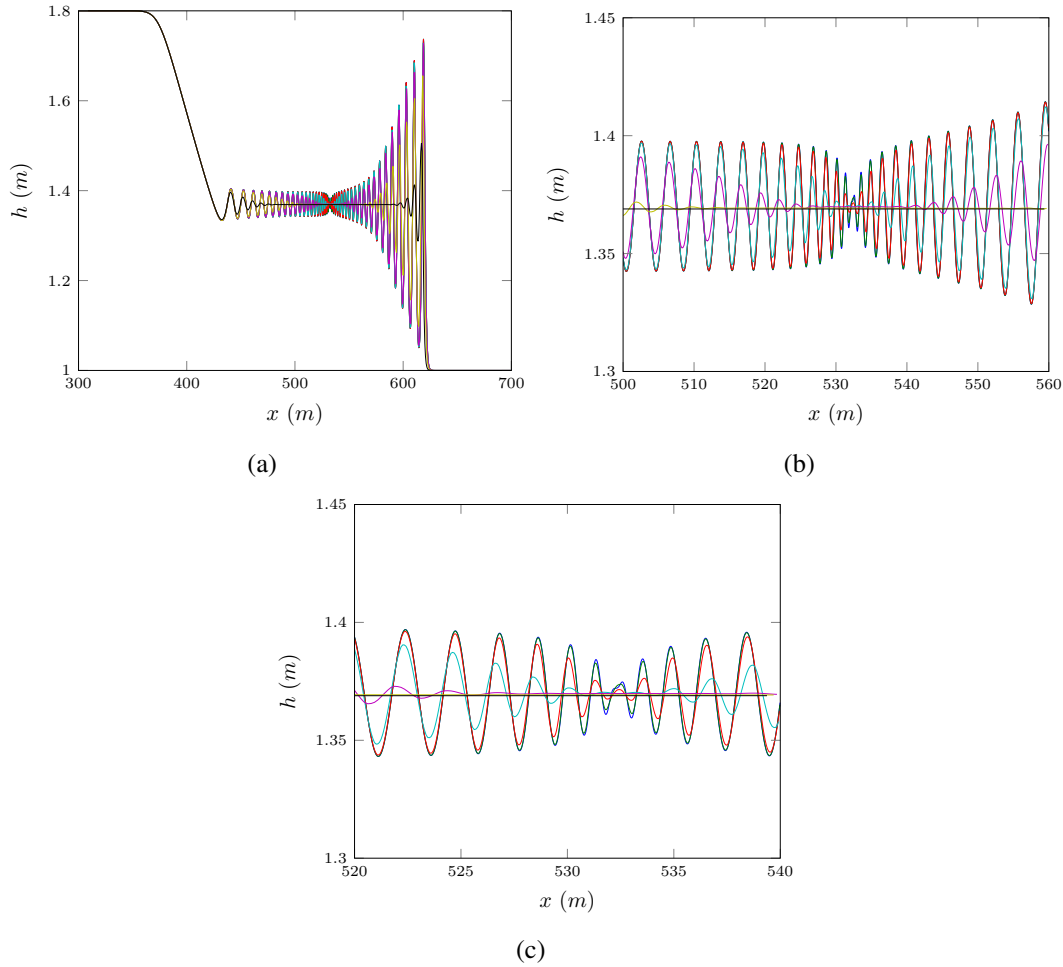


FIG. 4: Smooth dam break problem for o3 [] with  $\alpha = 2.5$  for  $\Delta x = 10/2^{10}$  (blue),  $\Delta x = 10/2^9$  (green),  $\Delta x = 10/2^8$  (red),  $\Delta x = 10/2^7$  (cyan),  $\Delta x = 10/2^6$  (magenta),  $\Delta x = 10/2^5$  (yellow),  $\Delta x = 10/2^4$  (black)

has hitherto not been presented and is certainly not an expected result. There are some important observations, changing  $\alpha$  does increase the height of the bump for the lowest resolution methods although after [] increasing  $\alpha$  has no effect[huh?]. The behaviour of these solutions in Figure 5 do not clearly show convergence, although it doesn't appear that there is a rapid divergence which suggests that this behaviour is not unstable. Also the lack of convergence is only around the contact discontinuity with other parts of the solution showing convergence.

All of the scenarios described above and displayed using the higher-order FDVM also

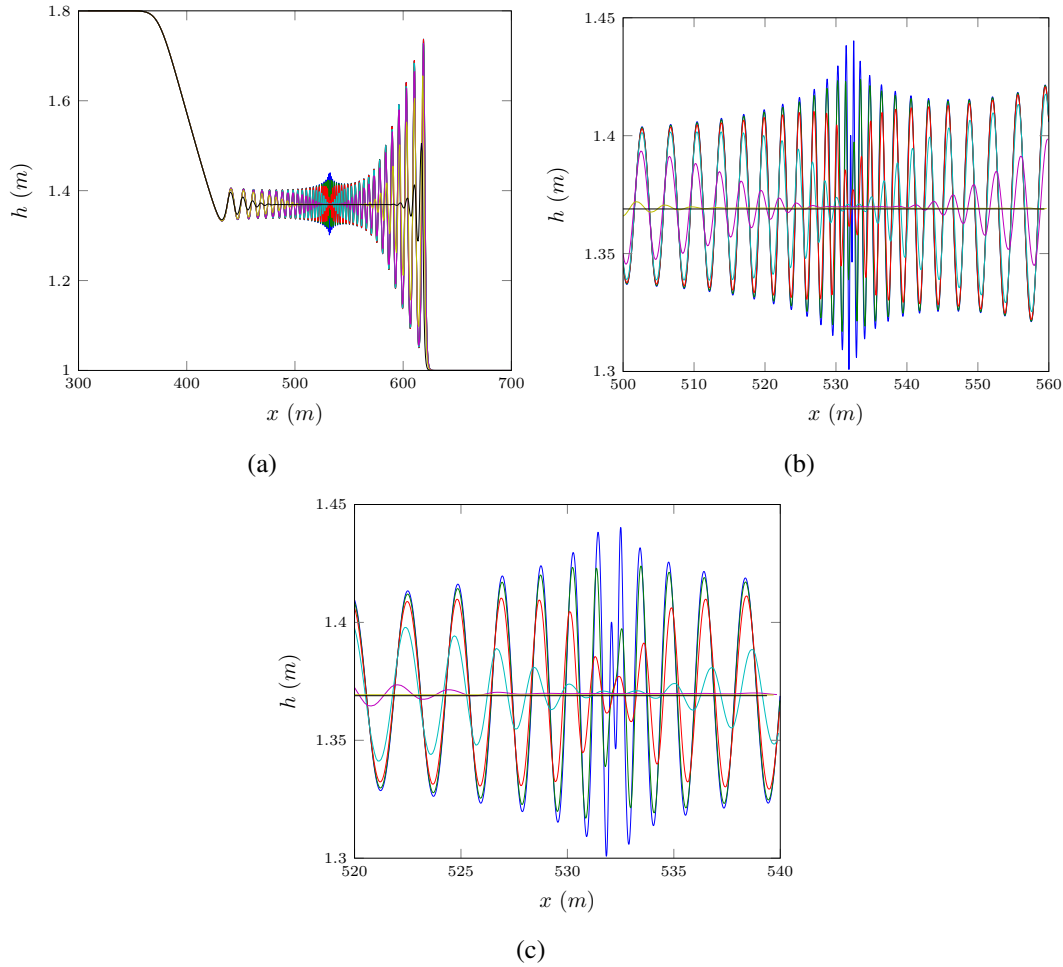


FIG. 5: Smooth dam break problem for o3 [] with  $\alpha = 1000.0$  for  $\Delta x = 10/2^{10}$  (blue),  $\Delta x = 10/2^9$  (green),  $\Delta x = 10/2^8$  (red),  $\Delta x = 10/2^7$  (cyan),  $\Delta x = 10/2^6$  (magenta),  $\Delta x = 10/2^7$  (yellow),  $\Delta x = 10/2^8$  (black)

occur for the FDM, however because finite differences cannot properly handle discontinuities this is a little more subtle. Firstly, since for each  $\alpha$  there is a  $\Delta x$  such that for larger  $\Delta x$  the smooth dam break problem is no longer smooth enough for a finite difference approximation to be appropriate. This becomes a problem for the contact discontinuity and bump scenarios since they require higher  $\alpha$  and are thus more discontinuous to begin with. The result of this are non-physical looking oscillations for large  $\Delta x$  values that were not replicated by the FDVM and thus can be attributed to this flaw of FDM as in Figure [].

Overall there were two types of trending behaviours as  $\Delta x$  was decreased one for the

271 FDM and another for the FDVM. FDM decreased the number of oscillations in the solution  
 272 as in Figure [], while FDVM increased the number of oscillations in the solution as can  
 273 be seen in Figure []. This is explained by Zoppou and Roberts (1996) as the FDM are  
 274 second order finite difference approximations their errors are dissipative thus introducing  
 275 oscillatory errors which are most prominent when  $\Delta x$  and therefore the errors are large.  
 276 While the behaviour of the FDVM is explained by a series of effects [] [TVD, treating  
 277 things as cell averages, thus flattening things in cells,].  
 278 [] (verify convergence rates near discontinuities?)

## 279 **Changing $\alpha$**

280 Increasing  $\alpha$  allows the initial conditions (7) to approach the dam break problem with  
 281  $h_1$  to the left and  $h_0$  to the right centred around  $x_0$ . So it would be expected that as  $\alpha \rightarrow \infty$   
 282 that the solution of the smooth dam break problem would approach the corresponding  
 283 dam break problem. This is the case for numerical methods because for a fixed  $\Delta x$   $\alpha$  can  
 284 be chosen large enough that (7) is precisely the dam break problem. This can be seen  
 285 in Figure [] with  $\Delta x =$  where the required  $\alpha$  for this to occur is below 1000 which was  
 286 the maximum  $\alpha$  value used in these experiments. However, only the FDVM were able to  
 287 handle such large  $\alpha$ 's because the initial conditions are not smooth enough to allow for  
 288 stability in the FDM as can be seen in Figure []. While the FDVM handled this quite well  
 289 and for all  $\Delta x$  tested as  $\alpha$  increased the solutions converged, even though for higher  $\Delta x$  []  
 290  $\alpha$  was not large enough to make (7) a jump discontinuity.

291 This confirms the superiority of the FDVM to handle non smooth initial conditions and  
 292 the inability of FDM to handle them. Even near discontinuous initial conditions caused  
 293 problems for the FDM with the introduction of oscillations that were not replicated by  
 294 the FDVM and appeared to be non-physical. An example of these transitional solutions  
 295 between the properly smooth initial conditions and the unstable discontinuous ones can be  
 296 seen in Figure []. [] (only compare the models when FD started smooth enough)

297 For the range of  $\alpha$ 's which are smooth enough for the FDM to be appropriate then as  
 298  $\alpha$  increases the number of oscillations increases as well for both the FDM and the FDVM.  
 299 So that the smoothness of the initial conditions controls the oscillations but this depends  
 300 on  $\Delta x$  since for a fixed  $\alpha$  the smoothness of the discretised initial conditions depends on  
 301  $\Delta x$ . [] (relative smoothness, more universal number)

302 It was observed that  $\Delta x$  can be chosen large enough such that increasing  $\alpha$  does not  
 303 resolve some of the more complex structure observed for smaller  $\Delta x$  values. This  $\Delta x$   
 304 depends on the model most notably for the first-order finite difference-volume scheme this  
 305  $\Delta x$  is very small. An example of this for the third-order FDVM scheme can be seen in  
 306 Figure [].

## Comparison of Models

The first-order FDVM was too diffuse and

## CONCLUSIONS

## ACKNOWLEDGEMENTS

## REFERENCES

- Carter, J. D. and Cienfuegos, R. (2011). "Solitary and cnoidal wave solutions of the Serre equations and their stability." *European Journal of Mechanics B/Fluids*, 30(3), 259–268.
- El, G., Grimshaw, R. H. J., and Smyth, N. F. (2006). "Unsteady undular bores in fully nonlinear shallow-water theory." *Physics of Fluids*, 18(027104).
- Kurganov, A., Noelle, S., and Petrova, G. (2002). "Semidiscrete central-upwind schemes for hyperbolic conservation laws and Hamilton-Jacobi equations." *Journal of Scientific Computing, Society for Industrial and Applied Mathematics*, 23(3), 707–740.
- Lannes, D. and Bonneton, P. (2009). "Physics of Fluids", 21(1), 16601–16610.
- Le Métayer, O., Gavriluk, S., and Hank, S. (2010). "A numerical scheme for the Green-Naghdi model." *Journal of Computational Physics*, 229(6), 2034–2045.
- Li, M., Guyenne, P., Li, F., and Xu, L. (2014). "High order well-balanced CDG-FE methods for shallow water waves by a Green-Naghdi model." *Journal of Computational Physics*, 257, 169–192.
- Mitsotakis, D., Dutykh, D., and Carter, J. (2014). "On the nonlinear dynamics of the traveling-wave solutions of the serre equations." *arXiv preprint arXiv:1404.6725*.
- Su, C. H. and Gardner, C. S. (1969). "Korteweg-de Vries equation and generalisations. III. Derivation of the Korteweg-de Vries equation and Burgers equation." *Journal of Mathematical Physics*, 10(3), 536–539.
- Zoppou, C. (2014). "Numerical solution of the One-dimensional and Cylindrical Serre Equations for Rapidly Varying Free Surface Flows." Ph.D. thesis, Australian National University, Australian National University.
- Zoppou, C. and Roberts, S. (1996). "Behaviour of finite difference schemes for advection diffusion equations." *Technical Report Mathematics Research Report No.MRR 062-96*.